PCCP

Accepted Manuscript

ROYAL SOCIETY OF CHEMISTRY

www.rsc.org/pccp

Controlling Phase Transition from Single-Layer MTe_2 (M=Mo, W): Modulation of Potential Barrier under Strain

H. H. Huang[a], Xiaofeng Fan[a, *], David J. Singh[a, c], Hong Chen [b],

Q. Jiang[a] and W.T. Zheng[a, †]

a. College of Materials Science and Engineering, Jilin University, Changchun 130012, China
b. Department of Control Science & Engineering, Jilin University, Changchun 130012, China
c. Department of Physics and Astronomy, University of Missouri, Columbia, Missouri 65211-7010, USA

*E-mail: xffan@jlu.edu.cn ; † E-mail: wtzheng@jlu.edu.cn

Abstract

Using first-principle DFT calculation, the path way and energy barrier of phase transition between 2H and 1T' has been investigated for monolayer $MoTe_2$ and WTe_2. The phase transition is controlled with the simultaneous movement of metal atoms and Te atoms in their plane without the intermediate phase 1T. The energy barrier (less than 0.9 eV per formula cell) is not so high that the phase transition is dynamically possible. The relative stability of both 2H and 1T' phase and energy barrier of phase transition can be modulated by the biaxial and uniaxial strain. The dynamical energy barrier is decreased by applying the strain. The phase transition between 2H and 1T' controlled by the strain can be used to modulate the electronic properties of $MoTe_2$ and WTe_2.

Keywords: Single-layer MTe_2, First-principle calculation, Phase transition, Energy barrier

1. Introduction

Group VI transition metal dichalcogenides (VI TMDs) with the chemical formula MX_2 have recently attracted much attention because of the superior physical properties and unique layered structure for potential application in electronic and optoelectronic devices[1-7]. These materials consist of X-M-X sheets which are held together via van der Waals interaction and can be thinned into single or few layers two-dimensional (2D) structure by several methods[8-11], such as liquid exfoliation and mechanical exfoliation with high crystal quality. Due to the lacking/change of layers' interaction, the electronic properties can be properly modulated. For example, bulk MoS_2 is an indirect band gap semiconductor with a band gap of 1.29 eV [12, 13], while single-layer MoS_2 is found to have a direct band gap of about 1.8 eV[14-16]. With strong photoluminescence, and controllable valley and spin polarization, 2D TMDs have aroused the interest in both the theoretical and experimental. Various studies, such as strain modulation and nanostructures, have addressed the tuning of band gaps and photoluminescence in MoS_2 and the related TMDs [17-26].

Phase transitions can modulate the properties of materials without the change of materials' composition and therefore are of important technological value. Most studies are focused on the hexagonal (2H) phase with semiconducting characteristic, while an overlooked feature is VI TMDs can exist in several polymorphs. Depending on the arrangement of X atoms[27], the other stable phase which is popular in VI TMDs is the distorted 1T phase (1T')[28-32]. 1T' phase has a trend of semimetal. For example, bulk 1T'-$MoTe_2$ is a semimetal with a much high carrier mobility of 4, 000 $cm^2V^{-1}s^{-1}$. The

metallic 1T'-WS_2 has the improved electrocatalytic activity[33]. The combining of 2H and 1T' phases with their special electronic characteristics will result in the potential applications in several areas, such as field effect transistor, batteries, photovoltaics and optoelectronics [2, 34, 35]. Some works about the structural transition between metallic 1T (or 1T') and semiconducting 2H phase including bulk materials and single layer has been done[36-38]. By the intercalation of Li and K, the 1T phase of MoS_2 transformed from 2H-MoS_2 with the contribution of electron donors was reported[8, 39]. However, bulk 1T-$LiMoS_2$ is thermodynamically unstable and can be transformed back to 2H phase, as the observed in Raman spectra[40]. Recently, in single-layer MoS_2, the coexistence of two phases has been reported by Eda *et al.*[10]. With scanning transmission electron microscopy, the structural transformation in single-layered MoS_2 is observed with atomic resolution by Lin *et al.*[41]. Theoretically, it is found that mechanical deformations can switch the thermodynamic stability between 2H phase and 1T' phase in the monolayer VI TMDs[42]. In addition, with an electron beam, it is found that 1T phase can be controllably grown in 2H phase for MoS_2. How about the dynamic barrier of phase transition between 2H and 1T' in VI TMD? As we all know, the related information about the dynamic processes of phase transition in these 2D materials still is limited.

In this work, we explored the mechanism of phase transition between 2H and 1T' of monolayer $MoTe_2$ and WTe_2 with first-principle methods. Both phases were considered to convert with each other by intra-layer atomic plane gliding. We analyzed the atomic moving mechanism in detail in order to obtain the information of phase transition pathway. It is found that the phase transition from 2H to 1T' is not simply by the

intermediate 1T phase with the plane gliding of X atom (Te) and the distortion of lattice. Actually, the mechanism is that the metal atom M (Mo or W) changes its position in the lattice of 2H phase to that in 1T' phase, simultaneously accompanied by the gliding of X (Te) atoms. In addition, in order to engineer the dynamic barrier of phase transition, we also analyzed the change of energy barrier under the strains including uniaxial and biaxial strain. The analysis of the dynamic process with energy barrier of phase transition in monolayer $MoTe_2$ and WTe_2 is expected to shed some light on the application of VI TMDs as 2D phase transition materials.

2. Calculation Methods

The $MoTe_2$ and WTe_2 are usually with 2H phase[43]. The 2H phase structure with space group *P-6m2* has hexagonal symmetry and the primitive unit cell of single-layer is three atoms. The X (Te) atom is with trigonal prismatic coordination around M (Mo or W) atoms. 1T phase is also with hexagonal symmetry and the primitive unit cell of single-layer is three atoms. In the 1T phase with space group *P-3m1*, the X atom is with octahedral coordination around M atoms. With previous study, the high symmetry 1T structure of single layer VI TMDs is thermodynamically unstable[44, 45], while another phase 1T', the distorted version of 1T phase, is found to be thermodynamically stable. This lower-symmetry phase is with space group *P21/M* and the primitive cell in *x*-*y* plane is rectangular[28]. In order to compare the structural change of three phases and perform the pathway analysis of phase transition, the 2H and 1T phase are constructed with rectangular supercell, as shown in Fig. 1 with that of 1T'. In the supercells of these single layer models, the vacuum separation in *z* direction is set to be 18 Å in order to avoid the

layers' coupling.

In present work, all the calculations were performed on the basis of density functional theory using accurate frozen-core full-potential projector augmented-wave pseudopotentials (PAW), as implemented in the VASP code[46]. We use the generalized gradient approximation (GGA) with the parameterization of Perdew-Burke-Ernzerhof (PBE) for the exchange and correlation potential[47]. In addition, we also consider the hybrid functional by using the HSE06 to accurately estimate the band gaps. A kinetic energy cutoff of 500 eV for the plane wave expansion and a Monkhorst-Pack grid with a k-point spacing of 0.02 $Å^{-1}$ are found to be sufficient to ensure that the total energy is converged at 1 meV/atom level. The convergence criterion for the self-consistence field energy was set to be 10^{-6} eV. In order to enable the initial structure to attain the most stable conformation, all the atomic positions and the lattice constants in *x*-*y* plane are fully relaxed.

3. Results and Discussion

3.1 Path Way and Barrier of Phase Transition

The lattice constants of monolayer $MoTe_2$ and WTe_2 with different phases, including 2H, 1T and 1T' phases are calculated and agreed well with the reported values from experiments and other theoretical calcualtions[42] as shown in Table 1. With our calculation, the ground states of $MoTe_2$ and WTe_2 are found to be 2H and 1T' phase, respectively. In addition, the energy of 1T phase is much higher than that of 2H and 1T' and the energy difference between 2H and 1T' is relatively small. From the view of atomic arrangement in the lattice, Mo (W) is coordinated by six Te atoms in three phases. However, the

coordinated structure is different. In the 2H, 1T and 1T' phase, the six Te atoms around Mo (W) are arranged with the trigonal prismatic, octahedral and distorted octahedral structure, respectively.

It is noticed that 1T phase can convert into the octahedral-like 1T' phase by a symmetry distortion. In the rectangular unit cell, the main difference between the two phases lies in the position of center metal atom as depicted in Fig. 1. Of course, the positions of Te atoms are modulated properly, by following the deviation of metal atom to the high symmetry position. For 1T structure, one of metal atoms is located in the middle of the cell (its coordinate corresponding to 0.5 along the *b*-axis), while this metal atom is below the central position for 1T' structure (its coordinate corresponding to 0.36 along the *b*-axis) in Fig. 1. Therefore, the path way from 1T to 1T' is that the metal atom (Mo or W) moves from the high symmetry position to a position deviated from the central in 1T' along the *y* axis of *x*-*y* plane (Fig. 2a) with the relaxation of Te atoms in the cell. From the calculation, it is found that there is no energy barrier from 1T to 1T'. In addition, one soft phonon mode in the optical modes of VI TMD materials which has an imaginary vibrational frequency has been found theoretically[42]. Is it possible that the phase transition from 2H to 1T' is completed by the intermediate phase 1T?

The coordinated structure can change from trigonal prismatic polytype to octahedral coordinated structure through the plane gliding of the atom layer of tellurium. This means the phase transition from 2H to 1T can be achieved by the moving of two Te atoms of one plane along *y* axis as shown in Fig. 2a. As the black lines in Fig. 2b and c shown, there is an energy barrier for from 2H to 1T, since Te atom needs to go through the center

between two Mo (W) atoms. The energy barriers for $MoTe_2$ and WTe_2 are 1.1 eV and 1.2 eV pre per formula unit, respectively. However, is it possible that the phase transition from 2H to 1T' is directly by the simultaneous moving of Mo (W) and Te with relative low energy barrier, but not via 1T phase, since there is no barrier between 1T and 1T' phase and the energy of 1T phase is higher?

In order to obtain the path way from 2H to 1T' with minimum energy barrier, we fix the metal atoms (Mo or W) on the special position (such as the center position of cell in 1T phase) and move Te atom from one equilibrium position to anther equilibrium position via the center of two metal atoms in the cell (Fig. 2a) as a special path way. Then by shifting the position of metal atom (Mo or W) to other special position along *y* axis indicated by the arrows in Fig. 2a and repeating the above process about the moving of Te atoms, we can obtain a series of energy curves. As shown in Fig. 2b and c which include the path ways of $MoTe_2$ and WTe_2 respectively, we can find the energy barriers of phase transition from 2H to 1T'. It should be noticed that the simultaneous displacement of Te atoms along *c*-axis by accompanying the Te plane slide along *b*-axis has been considered, since the coordinates of Te atoms on *c*-axis are different for both phases 2H and 1T'. The energy of 2H phase is taken as the zero point. For each curve with a fixed special position of Mo (W) atom, the energy increases with the Te atom going down along *b*-axis. When the Te atom arrive the center of both nearest-neighbor Mo (W) atoms, the energy reach the maximum. Then the energy will decline after the Te atom goes across the center between Mo (W) atoms. The energy appears a minimum value when the Te atom in a suitable position which is the local equilibrium point.

In the case of $MoTe_2$, the barrier of energy curve decreases gradually by following the shift of Mo along the *b*-axis. The barrier reaches the minimum when Mo atom is shifted to the position in 1T' phase in which the corresponding coordinate is 0.36 along *b*-axis as labeled in Fig. 2a. It is apparent that the 2H-1T phase transition might be unaccessible. For WTe_2, the similar results are obtained, as shown in Fig. 2c. The above calculations in Fig. 2b-c, in essence, are based on the analysis of two-step method about phase transition from 2H-1T'. In this method, for a fixed M atom position, we can obtain Te atom position on the reaction coordinate. For a given Te plane displacement on reaction coordinate, M atom position is determined by the lowest energy. In this way, the minimum energy path can be obtained. In addition, we just perform the calculations of two curves where the M atoms positions are fixed at the points 0.5 and 0.36 in *b*-axis to obtain the energy barrier from 2H to 1T'. Therefore, we can conclude that 2H-1T' phase transition is controlled by Mo and Te atom gliding simultaneously without going through the intermediate phase 1T. For $MoTe_2$ and WTe_2, the energy barriers are about 0.89 and 0.77 eV per formula cell, respectively.

The lattice parameters *a* and *b* in both phases 2H and 1T' are difference and the difference is about 1~1.5%, as shown in Table 1. By comparing the energy barriers calculated with the fixed lattice parameters from 2H and that from 1T', it is found that the difference is about 0.05 eV per formula cell in Table S1 in the ESI. To compare with the value of energy barrier itself, this error is small and the volume-fixed nudged elastic band in this work is enough to analyze this phase transition. From 2H to 1T', the lattice parameters *a* and *b* are not obviously changed. Therefore, this continuous model about the

displacements of the involved atoms with fixed lattice parameters *a* and *b* can be considered to be valid for this first order phase transition between 2H and 1T'. On the other side, if the distance of the Te atoms (as shown in Fig. 1) is considered to be as the reference of the lattice parameter in *c*-axis, this parameter of both phases is obviously discontinuous. In the phase transition of both phases, the change of this parameter is obvious and can be captured with the two-step method as shown in Fig. S1 in the ESI.

Experimentally, the electrically activated phase transitions between 1T' and 2H have been demonstrated in multilayer TaS_2 [48] and $TaSe_2$ [49]. In the monolayer VI TMD materials, the stress and strain could be applied via the deformation of flexible substrate and large elastic deformations can be reached through tensile strain. Therefore, the structure stability may be transformed by the mechanical deformation[50]. In order to realize the structure transition of monolayer telluride and gain a particular phase, we enable the independent control of lattice parameters to prove the structure transition and estimate the energy barrier.

3.2 Phase Transition under Biaxial Strain

From the above analysis, we can extract the dynamic energy barrier between 2H and 1T' from the curves of both initial and final states which are corresponded to the fixed position of metal atom at the points 0.5 and 0.36 in *b*-axis. As shown in Fig. 3a and 3b, the curves of initial and final states under biaxial tensile strain of 5%, 10% and 15% are shown for phase transition between 2H and 1T' of $MoTe_2$ and WTe_2, respectively. It is interesting that the curve of final state becomes flat by following the increase of tensile strain. This implies that the energy barrier will decrease with the increase of tensile strain.

In addition, it is noticed that the curve of finial state of $MoTe_2$ (shown by the green open circle line in Fig. 3a) under strain of 10% have a barrier with sharp peak and it implies there may be a transition of structural stability.

In Fig. 3c and d, the changes of energy barriers following the increase of tensile strain are shown for $MoTe_2$ and WTe_2. The changes of energy difference (ΔE) between 2H and 1T' phase due to the strain are also analyzed. The energy difference is calculated by the formula, $\Delta E = E_{2H} - E_{1T'}$, where E_{2H} and $E_{1T'}$ are the total energies of 2H and 1T phases, respectively. For $MoTe_2$, the ground state is 2H phase and the 1T' phase becomes more stable after the tensile strain reaches 10%. When the strain is less than 10%, the energy barrier is decreased by following the increase of strain. The change of relative stability of both phases under the strain of 10% results in the increase of energy barrier. Following the increase of strain further, the energy barrier between both phases is decreased again. For WTe_2, the energy difference between 2H and 1T' is increased and the energy barrier of both phases is decreased by following the increase of tensile strain. This means the phase transition from 2H to 1T' becomes easier with the increase of tensile strain. Here, it should be noticed that the 10% strain is possible to be near the upper boundary of MTe_2, since the breaking strain of the similar 2D materials, monolayer graphene and MoS_2 are about 12% and 11%, respectively[51, 52]. This implies that the biaxial strain may be not an effective way since the mechanical strain more than 10% is not easily achievable.

3.3 Phase Transition under Uniaxial Strain

In the experiments, the lattice parameters of the monolayer TMD may be tuned

independently by virtue of substrate. Here we consider the effect of uniaxial strain to phase transition by tuning the lattice parameter *b* and fixing the lattice parameter *a*. The relative energy-coordinate curves of both $MoTe_2$ and WTe_2 are displayed in Fig. 4a and 4b for the case of uniaxial tensile strain. It is found that the stability of 2H and 1T' is reversed for $MoTe_2$ beyond the critical uniaxial strain of 8%, as manifested in Fig. 4a. When this phase transition occurs under the uniaxial strain of 8%, the energy barrier is about 0.78 eV per formula unit (illustrated in Fig. 4c). In addition, the energy barrier is decreased continuously by following the increase of the uniaxial tensile strain. Therefore, the phase transition between 2H and 1T' is easier under uniaxial strain than under biaxial strain. In contrast to $MoTe_2$, there is no transition of structural stability observed for WTe_2 in Fig. 4d. Following the increase of the uniaxial tensile strain up to 8%, the 1T' phase becomes more stable than 2H. After the strain more than 8%, the energy difference between 1T' and 2H doesn't change obviously, while the energy barrier is decreased continuously by following the increase of strain.

It is noticed that the large uniaxial tensile strain along *b*-axis will induce the compression in *a*-axis. We considered the cases of $MoTe_2$ under the uniaxial tensile strain of *b*-axis with about 8%. It is found that the compression of *a*-axis is different under the tensile strain of *b*-axis for both phases. The *a*-axis compression of 1T' is larger than that of 2H. The tensile strain along *b*-axis for the reversion of phase stability between 2H to 1T' is reduced to about 6% with energy barrier of 0.782 eV per formula unit as shown in Fig. S2 in the ESI. The effect of the *a*-axis compression on the energy barrier of phase transition under the tensile strain of *b*-axis is checked. It is found that this effect on the

energy barrier is small and less than 0.03 eV per formula unit in Fig. S2-S3 and Table S2-S3 in the ESI.

We also perform the calculations about $MoTe_2$ and WTe_2 under the uniaxial compressive strain along *b*-axis with the fixed *a*-axis. As shown in Fig. 5a and c, the energy barrier between 2H and 1T' of $MoTe_2$ is decreased by following the increase of compressive strain, while the 2H phase is also more stable under compressive strain. This makes the phase transition from 2H to 1T' difficult under compressive strain. Interesting, the uniaxial compressive strain along *b* axis have an obvious impact on the phase transition of WTe_2, as shown in Fig. 5b and d. When the uniaxial compressive strain is less than 3%, the 1T' phase is more stable. After the compressive strain more than 3%, the 2H phase is more stable. When the phase transition from 1T' to 2H happens, the energy barrier is about 0.78 eV per formula unit. With the increase of compressive strain, the barrier strain will be decreased further. At the same time 2H phase is more stable than 1T' phase.

We also considered the effect of *a*-axis expansion under the uniaxial compressive strain of *b*-axis for WTe_2. It is found that the *a*-axis expansion of 2H is smaller than that of 1T' following the increase of *b*-axis compressive strain in Fig. S5 and Table S4 in the ESI. The effect of *a*-axis expansion on the energy barrier under the *b*-axis compressive strain is found to be small and can be ignored for WTe_2 as shown in Fig. S6 and Table S5 in the ESI.

3.4 Electronic Properties of Different Phases

Because of the coordinate structure difference, from the trigonal prismatic structure

to the distorted octahedral structure, both phases (2H and 1T') exhibit completely different electronic structures. We calculated the density of states (DOS) and band structures of unstrained monolayer $MoTe_2$ and WTe_2 with different phases including 2H, 1T and 1T' phase, as shown in Fig. 6 and 7. By PBE/GGA without spin-orbit coupling, the monolayer 2H-$MoTe_2$ and 2H-WTe_2 are found to be semiconductors with a direct band gap of 1.11 eV and 1.08 eV, respectively. The valence band maximum (VBM) and conduction band minimum (CBM) are located at the K-point of the Brillion zone and contributed from the *d* orbitals of metal atom (Mo and W). With considering the spin-orbit coupling, the bands near valance band maximum at K are splitted obviously (in Fig. S7 and Fig. S8 in the ESI). By considering the underestimate of PBE/GGA to the band gaps of semiconductors, the functional HSE06 is employed and these calculated results are shown in Table 2.

For 1T-$MoTe_2$ and 1T-WTe_2, the band gap of monolayer is closed and VBM and CBM are overlapped. After the structural distortion from 1T to 1T', the states near VBM and CBM have been changed to some extent (Fig. 6c and f) due to the low symmetry of crystal field. The states of valance band and that of conduction band aren't separated completely (Fig. 7c and f). Therefore, 1T'-$MoTe_2$ and 1T'-WTe_2 are with semimetal characteristic. However, with the considering of spin-orbit coupling and the more accurate underestimate of band gap by HSE06 functional, both the valance band and conduction band are separated for 1T'-$MoTe_2$ and 1T'-WTe_2 (in Fig. S9 in the ESI). It is consistent with the recent report about the band gap opening of monolayer 1T'-$MoTe_2$ by spin-orbit coupling[53]. This may make 1T'-$MoTe_2$ and 1T'-WTe_2 the potential application

on topological quantum devices.

4. Conclusion

In summary, the structural and electronic properties of the tellurides $MoTe_2$ and WTe_2 are studied by density functional theory calculations. It is found that phase transition between 2H and 1T' is controlled with the simultaneous movement of metal atoms and Te atoms in their plane and doesn't go through the intermediate state 1T phase. With the analysis of path way and dynamic energy barrier by the special two-step method, it is found that the phase transition is possible since the energy barrier is not high. The energy barriers of $MoTe_2$ and WTe_2 are about 0.89 eV and 0.77 eV per formula cell.

The relative stability of both 2H and 1T' phase can be modulated by the biaxial and uniaxial strain. The dynamical energy barrier is found to be decreased by applying the stress and strain. For $MoTe_2$, the phase transition from 2H to 1T' can be controlled by biaxial or uniaxial tensile strain. Under the biaxial tensile strain of 10%, 1T' phase becomes to be more stable than 2H phase and the energy barrier of both phases is 0.90 eV per formula unit. Under the *b*-axis tensile strain of about 6%, the 1T' phase become to be more stable and the energy barrier is 0.782 eV per formula cell. In addition, the energy barrier is decreased by following the increase of tensile stain further. For WTe_2, the phase transition from 1T' to 2H can be controlled by the uniaxial compressive strain along *b* axis. It is found that 2H phase becomes to be more stable than 1T' phase and the energy barrier is 0.78 eV per formula unit under the uniaxial compressive strain of about 3%. In addition, the 2H-1T' phase transition can induce the change of electronic properties. With $MoTe_2$ and WTe_2 as an example, it is expected that phase transition between 2H and 1T'

of VI TMD controlled by the strain can provide more applications for flexible, low-power and transparent electronic devices.

Acknowledgments
The support from the National Natural Science Foundation of China (No. 11504123) is highly appreciated.

Electronic supplementary information (ESI) available: Including the calculations about the effect of the change of lattice parameters on energy barrier, The changes of lattice paramerter along *c*-axis in the processes of phase trantion from 2H to 1T', the effect of *a*-axis compression under the *b*-axis tensile strain for $MoTe_2$ and the effect of *a*-axis expansion under b-axis compressive strain for WTe_2.

Reference

1. Brown, B. E., The Crystal Structures of WTe_2 and High-Temperature $MoTe_2$. *Acta Cryst.* **1966,** 20, 268.
2. Zeng, H.; Dai, J.; Yao, W.; Xiao, D.; Cui, X., Valley polarization in MoS_2 monolayers by optical pumping. *Nat. Nanotechnol.* **2012,** 7, 490.
3. Wang, Q. H.; Kalantar-Zadeh, K.; Kis, A.; Coleman, J. N.; Strano, M. S., Electronics and optoelectronics of two-dimensional transition metal dichalcogenides *Nat. Nanotechnol.* **2012,** 7, 699.
4. Terrones, H.; Lopez-Urias, F.; Terrones, M., Novel hetero-layered materials with tunable direct band gaps by sandwiching different metal disulfides and diselenides. *Sci. Rep.* **2013,** 3, 1549.
5. Radisavljevic, B.; A.Radenovic; Brivio, J.; Kis, A., Single-layer MoS_2 transistors. *Nat. Nanotechnol.* **2010,** 6, 147.
6. Novoselov, K. S.; Jiang, D.; Schedin, F.; Booth, T. J.; Khotkevich, V. V.; Morozov, S. V.; Geim, A. K., Two-dimensional atomic crystals. *Proc. Natl. Acad. Sci. USA* **2005,** 102, 10451-3.
7. Levi, R.; Bitton, O.; Leitus, G.; Tenne, R.; Joselevich, E., Field-effect transistors based on WS_2 nanotubes with high current-carrying capacity. *Nano Lett.* **2013,** 13, 3736.
8. Py, M. A.; Haering, R. R., Structural destabilization induced by lithium intercalation in MoS_2 and related compounds. *Can. J. Phys.* **1982,** 61, 76-84.
9. Coleman, J. N.; Lotya, M.; O'Neill, A.; Bergin, S. D.; King, P. J.; Khan, U.; Young, K.; Gaucher, A.; De, S.; Smith, R. J., Two-Dimensional Nanosheets produced by liquid exfoliation of layered materials. *Science* **2011,** 331, 568.

10. Eda, G.; Yamaguchi, H.; Voiry, D.; Fujita, T.; Chen, M.; Chhowalla, M., Photoluminescence from chemically exfoliated MoS_2. *Nano Lett.* **2011,** 11, 5111.

11. Yang, D.; Frindt, R. F., Li-intercalation and exfoliation of WS_2. *J. Phys. Chem. Solids* **1995,** 57, 1113.

12. Böker, T.; Severin, R.; Müller, A.; Janowitz, C.; Manzke, R.; Voß, D.; Krüger, P.; Mazur, A.; Pollmann, J., Band structure of MoS_2,$MoSe_2$,andα−$MoTe_2$:Angle-resolved photoelectron spectroscopy andab initiocalculations. *Phys. Rev. B* **2001,** 64, 235305.

13. Conan, A.; Bonnet, A.; Amrouche, A.; Spiesser, M., Semiconducting properties and band structure of $MoTe_2$ single crystals. *J. Physique.* **1984,** 45, 459.

14. Liu, G.-B.; Xiao, D.; Yao, Y.; Xu, X.; Yao, W., Electronic structures and theoretical modelling of two-dimensional group-VIB transition metal dichalcogenides. *Chem. Soc. Rev.* **2014,** 44, 2643-2663.

15. Mak, K. F.; Lee, C.; Hone, J.; Shan, J.; Heinz, T. F., Atomically Thin MoS_2: A New Direct-Gap Semiconductor. *Phys. Rev. Lett.* **2010,** 105, 136805.

16. Zhuang, H. L.; Johannes, M. D.; Blonsky, M. N.; Hennig, R. G., Computational prediction and characterization of single-layer CrS_2. *Appl. Phys. Lett.* **2014,** 104, 022116.

17. Amin, B.; Kaloni, T. P.; Schwingenschlogl, U., Strain engineering of WS_2, WSe_2, and WTe_2. *RSC Adv.* **2014,** 4, 34561.

18. Debbichi, L.; Eriksson, O.; Lebègue, S., Electronic structure of two-dimensional transition metal dichalcogenide bilayers from *ab initio* theory. *Phys. Rev. B* **2014,** 89, 205311.

19. Güller, F.; Llois, A. M.; Goniakowski, J.; Noguera, C., Prediction of structural and metal-to-semiconductor phase transitions in nanoscaleMoS_2,WS_2, and other transition metal dichalcogenide zigzag ribbons. *Phys. Rev. B* **2015,** 91, 075407.

20. Yun, W. S.; Han, S. W.; Hong, S. C.; Kim, I. G.; Lee, J. D., Thickness and strain effects on electronic structures of transition metal dichalcogenides: 2H-MX_2semiconductors (M=Mo, W;X=S, Se, Te). *Phys. Rev. B* **2012,** 85, 033305.

21. Yanfeng Chen; Xi, J.; Dumitru O. Dumcenco; Liu, Z.; Suenaga, K.; DongWang; Zhigang Shuai; Huang, Y.-S.; Xie, L., Tunable Band Gap Photoluminescence from Atomically Thin Transition-Metal Dichalcogenide Alloys. *ACS Nano* **2013,** 7, 4610.

22. Kaul, A. B., Two-dimensional layered materials: Structure, properties, and prospects for device applications. *J. Mater. Res.* **2014,** 29, 348.

23. Fan, X.; Chang, C. H.; Zheng, W. T.; Kuo, J.-L.; Singh, D. J., The electronic properties of single-layer and multilayer MoS_2 under high pressure. *J. Phys. Chem. C* **2015,** 119, 10189-10196.

24. Feng, J.; Qian, X.; Huang, C.-W.; Li, J., Strain-engineered artificial atom as a broad-spectrum solar energy funnel. *Nat Photon* **2012,** 6, 866-872.

25. Conley, H. J.; Wang, B.; Ziegler, J. I.; Haglund, R. F.; Pantelides, S. T.; Bolotin, K. I., Bandgap Engineering of Strained Monolayer and Bilayer MoS2. *Nano Lett.* **2013,** 13, 3626-3630.

26. Lu, N.; Guo, H.; Li, L.; Dai, J.; Wang, L.; Mei, W.-N.; Wu, X.; Zeng, X. C., MoS2/MX2 heterobilayers: bandgap engineering via tensile strain or external electrical field. *Nanoscale* **2014,** 6, 2879-2886.

27. Clarke, R.; Marseglia, E.; Hughes, H. P., A low-temperature structural phase transition in β-$MoTe_2$. *Philos. Mag. B* **1978,** 38, 121.

28. Dawson, W. G.; Bullett, D. W., Electronic structure and crystallography of $MoTe_2$ and WTe_2. *J. Phys. C: Solid State Phys.* **1987,** 20, 6159.

29. Heising, J.; Kanatzidis, M. G., Structure of Restacked MoS_2 and WS_2 Elucidated by Electron Crystallography. *J. Am. Chem. Soc.* **1999,** 121, 638.

30. Hla, S. W.; Marinkovic, V.; Prodan, A.; Musevic, I., STM/AFM investigations of β-$MoTe_2$, a-$MoTe_2$ and

WTe_2. *Surf. Sci.* **1996,** 352, 105-111.

31. Wypych, F.; Weber, T.; Prins, R., Scanning Tunneling Microscopic Investigation of 1T-MoS_2. *Chem. Mater.* **1998,** 10, 723.

32. Revolinsky, E.; Bebrntsen, D. J., Electrical properties of a- and β- $MoTe_2$ as affected by stoichiometry and preparation temperature. *J. Phys. Chem. Solids* **1966,** 27, 523-526.

33. Voiry, D.; Yamaguchi, H.; Li, J.; Silva, R.; Alves, D. C. B.; Fujita, T.; Chen, M.; Asefa, T.; Shenoy, V. B.; Eda, G.; Chhowalla1, M., Enhanced catalytic activity in strained chemically exfoliatedWS_2 nanosheets for hydrogen evolution. *Nat. Mater.* **2013,** 12, 850.

34. Mak, K. F.; He, K.; Shan, J.; Heinz, T. F., Control of valley polarization in monolayer MoS_2 by optical helicity. *Nat. Nanotechnol.* **2012,** 7, 494.

35. Lembke, D.; Bertolazzi, S.; Kis, A., Single-layer MoS_2 electronics. *Acc. Chem. Res.* **2015,** 48, 100.

36. Ambrosi, A.; Sofer, Z. k.; Pumera, M., 2H - 1T phase transition and hydrogen evolution activity of MoS_2, $MoSe_2$, WS_2 and WSe_2 strongly depends on the MX_2 composition†.pdf. *Chem. Commun.* **2015,** 51, 8450-8453.

37. Bhattacharyya, S.; Singh, A. K., Semiconductor-metal transition in semiconducting bilayer sheets of transition-metal dichalcogenides. *Phys. Rev. B* **2012,** 86, 075454.

38. Wang, H.; Yu, L.; Lee, Y. H.; Shi, Y.; Hsu, A.; Chin, M. L.; Li, L. J.; Dubey, M.; Kong, J.; Palacios, T., Integrated circuits based on bilayer MoS_2 transistors. *Nano Lett.* **2012,** 12, 4674-80.

39. Mattheiss, L. F., Band Structures of Transition-Metal-Dichalcogenide Layer Compounds. *Phys. Rev. B* **1973,** 8, 3719.

40. Sandoval, S. J.; Yang, D.; Frindt, R. F.; Irwin, J. C., Raman study and lattice dynamics of single molecular layers of MoS_2. *Phys. Rev. B* **1991,** 44, 3955-3962.

41. Lin, Y.-C.; Dumcenco, D. O.; Huang, Y.-S.; Suenaga, K., Atomic mechanism of the semiconducting to metallic phase transition in single-layered MoS_2. *Nat. Nanotechnol.* **2014,** 9, 391.

42. Duerloo, K. A.; Li, Y.; Reed, E. J., Structural phase transitions in two-dimensional Mo- and W-dichalcogenide monolayers. *Nat. Commun.* **2014,** 5, 4214.

43. Yang, D.; Sandoval, S. J.; Divigalpitiya, W. M. R.; Irwin, J. C.; Frindt, R. F., Structure of single-molecular-layerMoS_2. *Phys. Rev. B* **1991,** 43, 12053.

44. Gordon, R. A.; Yang, D.; Crozier, E. D.; Jiang, D. T.; Frindt, R. F., Structures of exfoliated single layers ofWS_2,MoS_2,and $MoSe_2$ in aqueous suspension. *Phys. Rev. B* **2002,** 65, 125407.

45. Nayak, A. P.; Pandey, T.; Voiry, D.; Liu, J.; Moran, S. T.; Sharma, A.; Tan, C.; Chen, C. H.; Li, L. J.; Chhowalla, M.; Lin, J. F.; Singh, A. K.; Akinwande, D., Pressure-dependent optical and vibrational properties of monolayer molybdenum disulfide. *Nano Lett.* **2015,** 15, 346.

46. Kresse, G.; Furthmuller, J., Efficient iterative schemes for ab initio total-energy calculations using a plane-wave basis set. *Phys. Rev. B* **1996,** 54.

47. Perdew, J. P.; Burke, K.; Ernzerhof, M., Generalized Gradient Approximation Made Simple. *Phys. Rev. Lett.* **1996,** 77, 4.

48. Kim, J.-J.; Park, C., Observation of a phase transition from the T phase to the H phase induced by a STM tip in 1T-TaS_2. *Phys. Rev. B* **1997,** 56, R15573.

49. Zhang, J.; Liu, J.; Huang, J. L.; kim, P.; Lieber, C. M., Creation of nanocrystals through a solid-solid phase transition induced by an STN tip. *Science* **1996,** 274, 757.

50. Fan, X.; Zheng, W. T.; Kuo, J. L.; Singh, D. J., Structural stability of single-layer MoS_2 under large strain. *J. Phys. Condens. Matter* **2015,** 27, 105401.

51. Bertolazzi, S.; Brivio, J.; Kis, A., Stretching and Breaking of Ultrathin MoS2. *ACS Nano* **2011,** 5,

9703-9709.

52. Lee, C.; Wei, X.; Kysar, J. W.; Hone, J., Measurement of the Elastic Properties and Intrinsic Strength of Monolayer Graphene. *Science* **2008,** 321, 385-388.

53. Keum, D. H.; Cho, S.; Kim, J. H.; Choe, D.-H.; Sung, H.-J.; Kan, M.; Kang, H.; Jae-YeolHwang; Kim, S.; Yang, H.; Chang, K. J.; Lee, Y. H., Bandgap opening in few-layered monoclinic $MoTe_2$. *Nature Physics* **2015,** 11, 482.

54. Puotinen, D.; Newnham, R. E., The crystal structure of $MoTe_2$. *Acta Cryst.* **1961,** 14, 691.

55. Huang, Y. L.; Chen, Y.; Zhang, W.; Quek, S. Y.; Chen, C.-H.; Li, L.-J.; Hsu, W.-T.; Chang, W.-H.; Zheng, Y. J.; Chen, W.; Wee, A. T. S., Bandgap tunability at single-layer molybdenum disulphide grain boundaries. *Nat Commun* **2015,** 6, 6298.

56. Vellinga, M. B.; Jonge, R. D.; Haas, C., Semiconductor to metal transition in $MoTe_2$. *J. Solid State Chem.* **1970,** 2, 299.

Table 1

Table 1. Calculated lattice parameters and formation energies for monolayer $MoTe_2$ and WTe_2 with different phases. Note that the lattice parameters *a* and *b* are from rectangular supercell with two formula units. The lattice parameter C is for the length of the X-M-X sandwich and the C of 1T' phase has two values (C_1 and C_2 shown in Figure 1c).

Materials	Stru.	a (Å)	b (Å)	C (Å)	ΔE(eV/atom)
$MoTe_2$	2H	3.548	6.146	3.595	-3.14
		3.519(Ref.28, 54)			
		3.550(Ref.55)	6.149		
		3.522(Ref. 12)			
	1T	3.493	6.048	3.730	-2.97
		3.493(Ref. 55)	6.054		
	1T'	3.454	6.365	2.956, 4.126	-3.12
		3.469(Ref. 30)	6.330		
		3.455(Ref. 55)	6.380		
WTe_2	2H	3.554	6.152	3.621	-3.27
		3.600(Ref. 28)			
		3.552(Ref. 55)	6.154		
	1T	3.517	6.091	3.740	-3.09
		3.491(Ref. 55)	6.320		
	1T'	3.496	6.311	2.951, 4.187	-3.30
		3.496(Ref. 30)	6.282		

Table 2

Table 2 Calculated band gap and spin-orbit coupling (Δ_{SOC}) of valance band maximum at K for monolayer 2H-$MoTe_2$ and 2H-WTe_2 with PBE and HSE06

Methods	$MoTe_2$		WTe_2	
	Gap (eV)	Δ_{SOC} (eV)	Gap (eV)	Δ_{SOC} (eV)
PBE without SOC	1.11	–	1.08	–
PBE with SOC	0.942	0.216	0.745	0.486
HSE without SOC	1.500	–	1.477	–
HSE with SOC	1.247	0.362	0.985	0.720
Ref. 13, 56	0.98, 1.18			

Figure 1

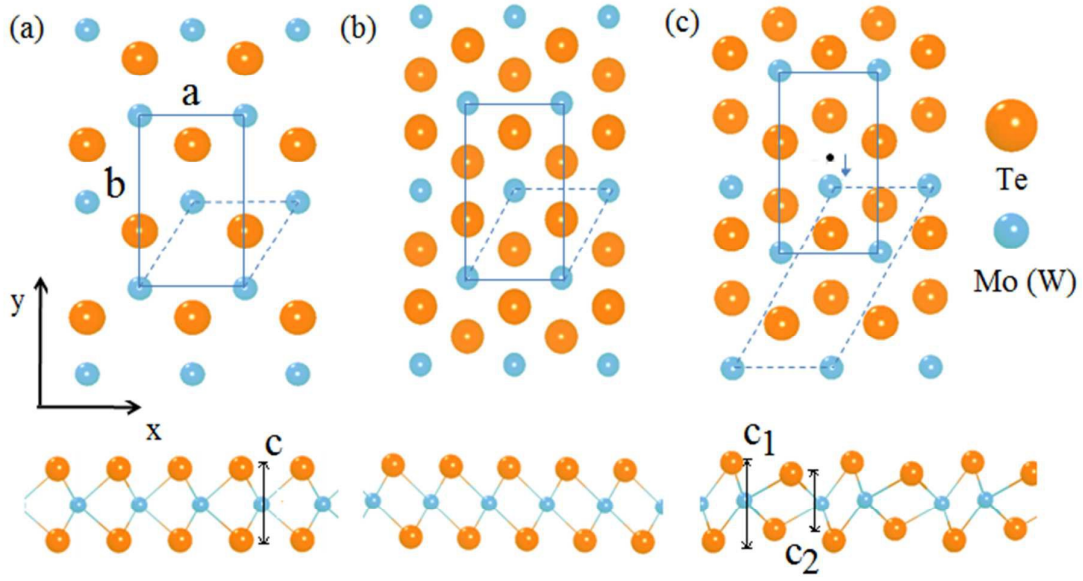

Fig.1. Schematic representation of the structures of different phases including 2H (a), 1T (b) and 1T' (c) for $MoTe_2$ and WTe_2.

Figure 2

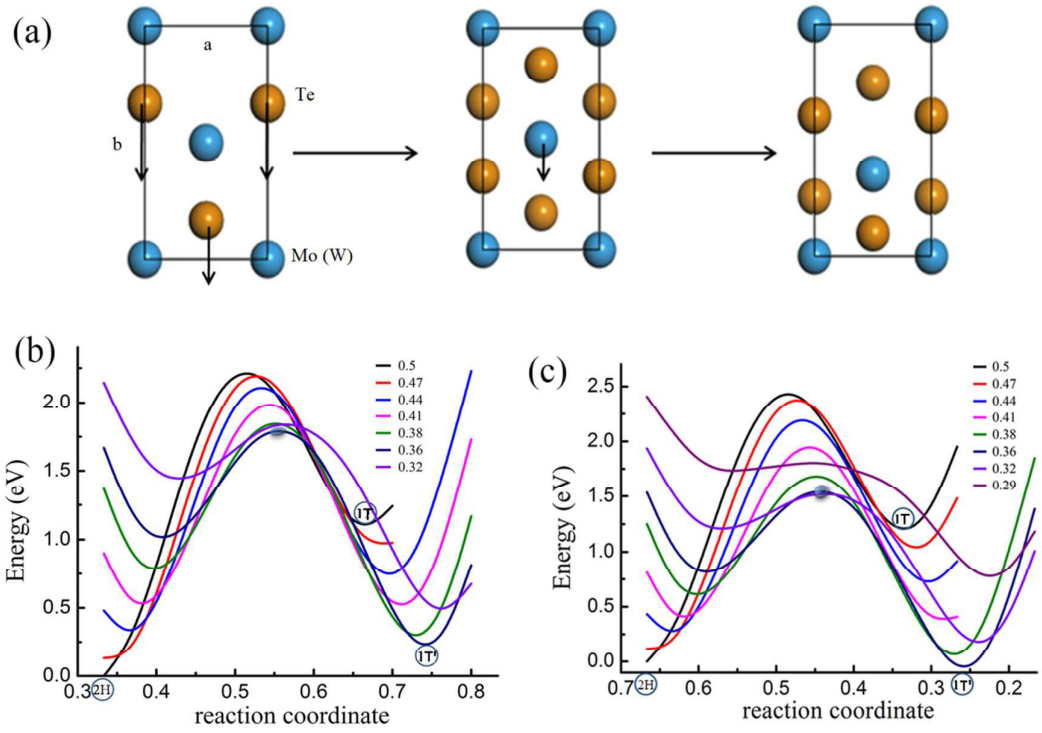

Fig. 2 Structure phase transition: possible path way of phase transition from 2H to 1T' by the intermediate phase 1T (a), and potential energy curves of different path ways with the movement of Te atoms and special fixed positions of metal atom from 0.5 to 0.32 in *b* axis for $MoTe_2$ (b) and WTe_2 (c). Note that arrows in (a) represent the direction of motion of Te atoms in 2H phase and metal atom in 1T' phase, all the energies are relative to that of 2H phase in (b) and (c), shadow point presents the energy barrier from 2H to 1T' in (b) and (c).

Figure 3

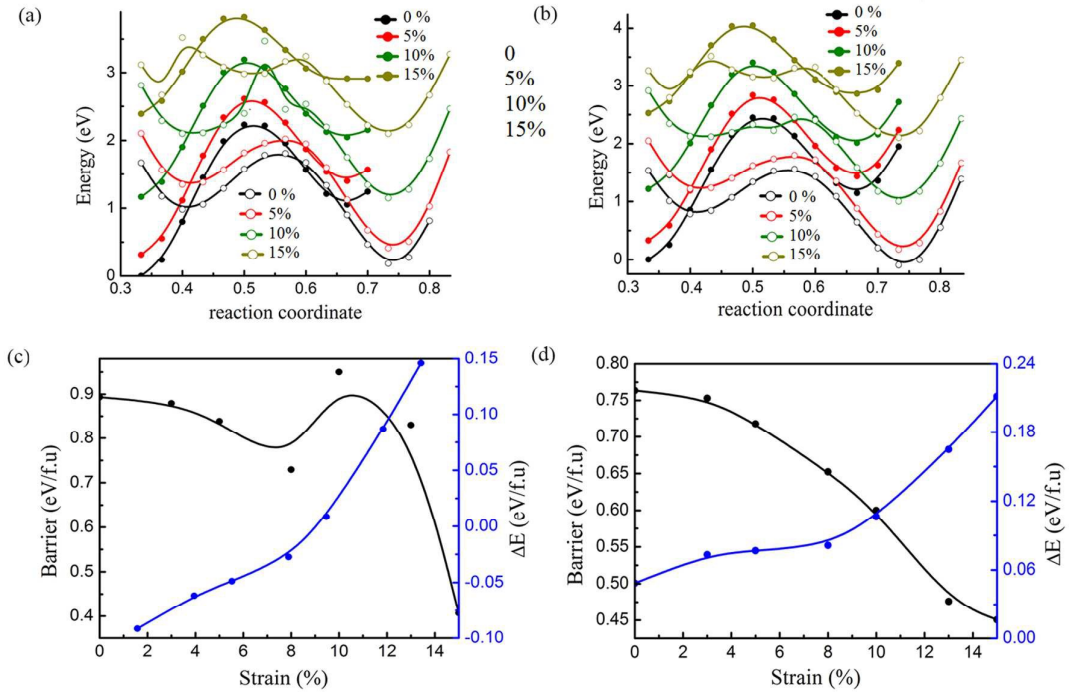

Fig.3 Phase transition under biaxial strain: potential energy curves of initial state (metal atom fixed at 0.5 in *b* axis shown by solid circle lines) and final state (metal atom fixed at 0.36 in *b* axis shown by open circle lines) under different strains up to 15% for $MoTe_2$ (a) and WTe_2 (b), and energy barrier (black line) and energy difference (blue line) as a function of strain for $MoTe_2$ (c) and WTe_2 (d).

Figure 4

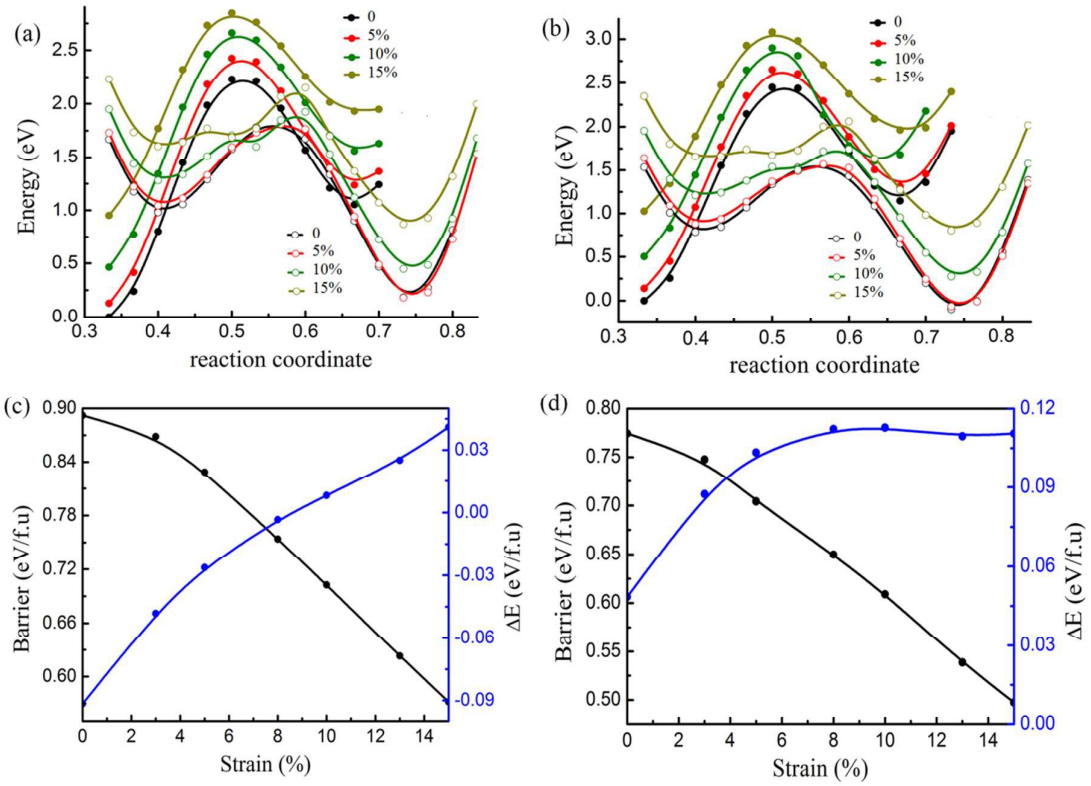

Fig.4 Phase transition under uniaxial tensile strain along *b* axis: potential energy curves of initial state (metal atom fixed at 0.5 in *b* axis shown by solid circle lines) and final state (metal atom fixed at 0.36 in *b* axis shown by open circle lines) under different strains up to 15% for $MoTe_2$ (a) and WTe_2 (b), and energy barrier (black line) and energy difference (blue line) as a function of strain for $MoTe_2$ (c) and WTe_2 (d).

Figure 5

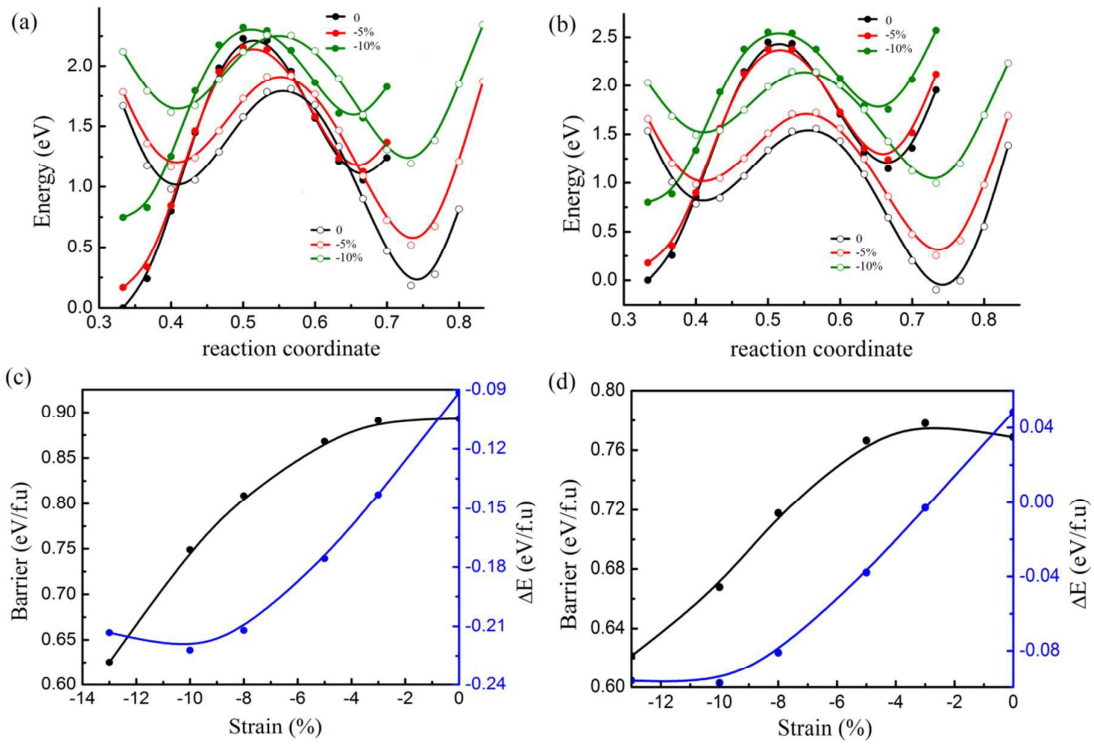

Fig.5 Phase transition under uniaxial compressive strain along *b* axis: potential energy curves of initial state (metal atom fixed at 0.5 in *b* axis shown by solid circle lines) and final state (metal atom fixed at 0.36 in *b* axis shown by open circle lines) under different strains up to 15% for $MoTe_2$ (a) and WTe_2 (b), and energy barrier (black line) and energy difference (blue line) as a function of strain for $MoTe_2$ (c) and WTe_2 (d).

Figure 6

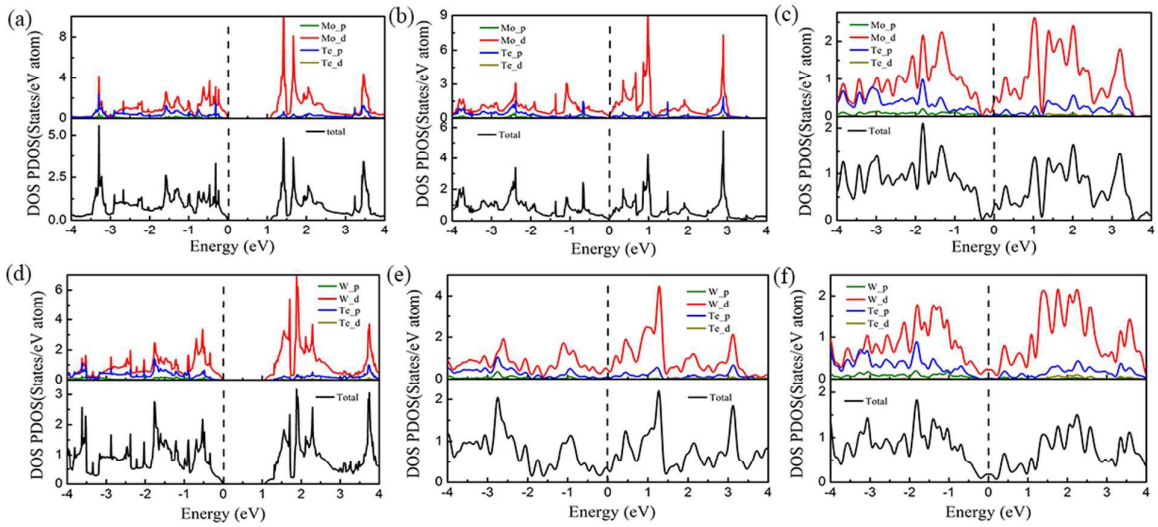

Fig.6 Density of states (DOS) and partial density of states (PDOS) of monolayer $MoTe_2$ with 2H (a), 1T (b) and 1T' (c) phase and that of monolayer WTe_2 with 2H (d), 1T (e) and 1T' (f) phase. Note the perpendicular dashed line at 0 eV denotes the Fermi level.

Figure 7

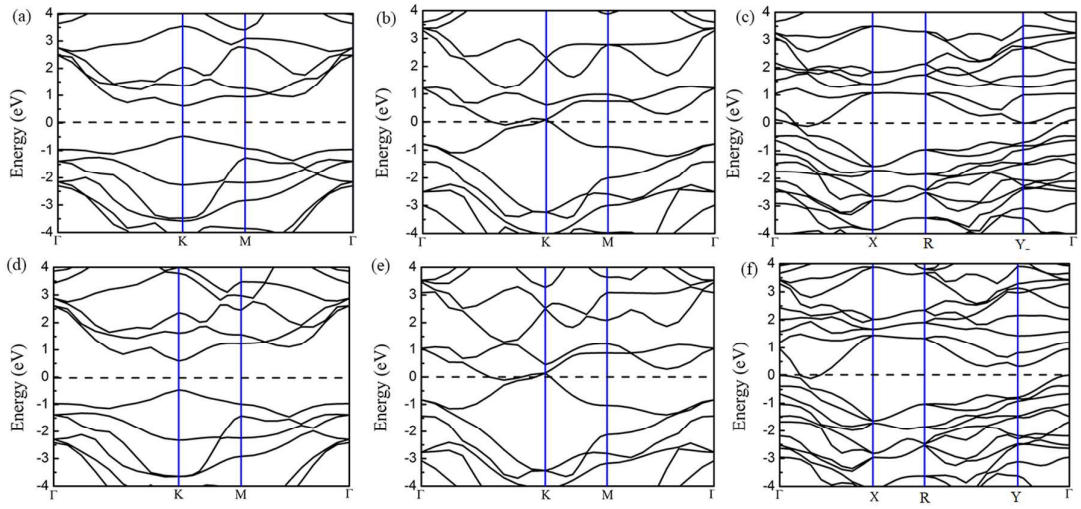

Fig.7 Electronic band structures of monolayer $MoTe_2$ with 2H (a), 1T (b) and 1T' (c) phase and that of monolayer WTe_2 with 2H (d), 1T (e) and 1T' (f) phase. Note that the horizontal dashed line at 0 eV denotes the Fermi level and R present for the high symmetry k-points (0.5, 0.5 0) in the Brillouin zone.

A table of contents entry: